Theory and characteristics of holographic polymer dispersed liquid crystal transmission grating with scaffolding morphology

Wenbin Huang,[1,2] Yonggang Liu,[1] Zhihui Diao,[1,2] Chengliang Yang,[1] Lishuang Yao,[1] Ji Ma,[3] and Li Xuan[1,*]

[1]State Key Laboratory of Applied Optics, Changchun Institute of Optics, Fine Mechanics and Physics, Chinese Academy of Sciences, Changchun 130033, China

[2]Graduate School of Chinese Academy of Sciences, Beijing 100039, China

[3]Liquid Crystal Institute, Kent State University, Kent, Ohio 44240, USA

*Corresponding author: xuanli@ciomp.ac.cn

Received 22 February 2012; revised 7 April 2012; accepted 10 April 2012; posted 10 April 2012 (Doc. ID 163341); published 12 June 2012

We have performed a detailed characterization of the optical properties of a holographic polymer dispersed liquid crystal (LC) transmission grating with polymer scaffolding morphology, which was fabricated with conventional high-functionality acrylate monomer under low curing intensity. Temporal evolution of the grating formation was investigated, and the amount of phase-separated LC was determined by birefringence investigation. A grating model combined with anisotropic coupled-wave theory yielded good agreement with experimental data without any fitting parameter. The results in this study demonstrate the non droplet scaffolding morphology grating is characterized by a high degree of phase separation (70%), high anisotropy, low scattering loss (<6%), and high diffraction efficiency (95%).

OCIS codes: 050.1950, 090.2890, 160.3710, 260.1440.

1. Introduction

Holographic polymer dispersed liquid crystals (HPDLCs) are electrically switchable photonic components with a great potential for electro-optical applications such as light switches [1], lenses [2,3], flat-panel displays [4], and distributed feedback waveguide lasers [5–7]. HPDLC gratings are fabricated by exposing a mixture composed of light-sensitive monomer and liquid crystal (LC) to an interference field created by two or multiple coherent light beams. In general, polymer is formed mainly in the bright patterns due to the free-radical polymerization, while monomer in the dark fringes diffuses to the bright fringes and LC in the bright region is squeezed out to the dark region. Therefore a stratified composite with alternating layers of polymer and LC corresponding to the interference patterns is formed.

Depending on different compositions of the prepolymer syrup and fabrication conditions, HPDLCs can exhibit different morphologies and electro-optical properties. The droplet-like morphology [8–14] transmission grating has been observed both in acrylate monomer and thiol-ene monomer, in which distinct, elongated-shaped droplets of LC are formed after phase separation. The diameter of LC droplets is approximately half the grating pitch, and the diffractive property of the grating is governed by the LC arrangement inside each droplet and the average director of all droplets. The diffraction efficiency (DE) of the grating is high, but the scattering loss is also high as the LC droplet size is comparable to visible wavelengths [15]. Another grating fabricated at a temperature above the LC clearing point with thiol-ene-based material has a slice-like morphology, in

which pure and well-aligned nematic LC is separated by polymer slices (so called POLICRYPS) [16]. The POLICRYPS grating shows great potential in various applications due to low scattering loss [17,18]. The third grating with low-functional acrylate monomer has a scaffolding-like morphology in which non droplet, phase-separated LC undergoes an additional interaction with polymer filaments across the polymer walls [19]. The employment of low-functional monomer [20] is thought to be the reason for the scaffolding morphology.

Optical properties of HPDLCs are strongly related to the grating morphology. In the models for the droplet-like morphological grating, a fitting dielectric tensor modulation was used to investigate the mean director of LC droplets [9]. Asystematic analysis of LC droplet orientation through fitting the diffractive curve was also implemented [10,21], and the permittivity modulation tensor and degree of phase separation were accessed by analyzing the angular dependence of the diffraction efficiency in a nano-sized droplet morphology grating [22].Random scattering was also incorporated in the model for the thiol-ene—based reflection grating [23]. For the slice-like morphologic grating, a Kogelnik-like model has been implemented to account for the temperature dependence of the diffraction efficiency [24].A numerical method has been used for both normal and conical incidence characterization of the POLICRYPS gratings [25]. However, the research of characterization on the scaffolding-like grating remains very limited. The aim of this work is to present a more thorough understanding of the forming mechanism of the scaffolding morphological grating and its peculiar optical properties. Through our theory and characterization, agreement between the prediction by anisotropic coupled-wave theory and experimental data was achieved. Further, the theoretical model presented here does not use any fitting parameter; thus it provides a more direct understanding of the grating structure. The reliability of our model was also confirmed by checking various samples with different grating pitch and phase-separation degree.

2. Experiment

Our HPDLC gratings were fabricated using an emulsion mixture containing 34 wt.% nematic LC (TEB30A, Slichem), whose n_o is 1.522 and n_e is 1.692; 54 wt.% monomer dipentaerythrol-hydroxyl-penta-acrylate (DPHPA; Sigma-Aldrich); 10 wt.% cross-linking stabilizer monomer *N*-vinylpyrrolidinone (NVP; Sigma-Aldrich); 0.5 wt.% photoinitiator Rose Bengal (RB; Sigma-Aldrich); and 1.5 wt.% coinitiator *N*-phenylglycine (NPG; Sigma-Aldrich). LC cells were made by two glass plates with a cell gap of 6.5 μm. The emulsion mixture was injected into the empty cells and irradiated undera 532 nm wavelength laser.

The experimental setup is schematically shown in Fig. 1. The light from a Nd-YAG laser at 532 nm wavelength was split into two beams that were directed onto the sample symmetrically with respect to the normal. In order to form different grating pitch, the intersecting angles were varied from 24° to 60°. The curing intensity of each beam was 4 mW/cm^2, which was sufficiently low compared with the droplet-like morphological grating forming condition, and the curing duration was controlled as 3 min. Exposure temperature was 25 °C. To monitor the diffracted light at different polarization states in real time, a circularly polarized light from a He-Ne laser-1 at 633 nm was incident onto the sample at the Bragg angle. The diffracted light was separated into *s* and *p* polarization components by a polarization beam splitter (PBS) before being detected by detector 2 (D2) and detector 3 (D3). The calibrated total incident light intensity for each polarization state was determined prior to the grating curing process. To calculate scattering loss of the grating during the fabrication process, a He-Ne laser-2 was directed onto the sample at normal direction and monitored. The transmissivity before recording was noted as a reference to calibrate the reflection loss caused by air-glass interface.

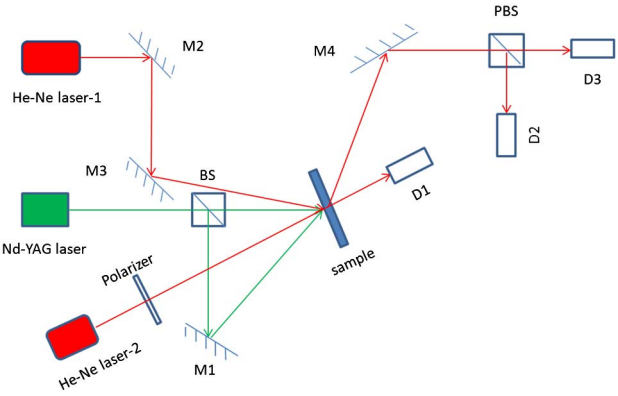

Fig. 1. (Color online) Schematic diagram of the setup for the curing process. D, detector; M, mirror; BS, beam splitter; PBS, polarization beam splitter.

After being recorded by the 532 nm laser, the sample was further exposed under a UV light source for 5 min to stabilize the scaffolding structure. Polarization optical microscopy (POM) and atomic force microscope (AFM) were used to explore the resulting morphology. For the AFM test, the sample was flushed with alcohol for 5 min to remove the LC. The LC birefringence in the grating was measured by the setup shown in Fig. 2. Light from a He–Ne laser

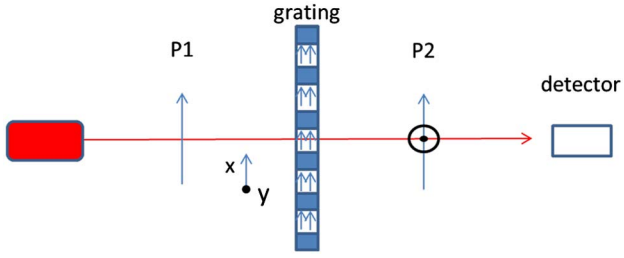

Fig. 2. (Color online) Experimental setup for the measurement of the grating birefringence. P1 and P2 are *x*-axis aligned and *y*-axis aligned polarizers.

(spot diameter 2 mm, power 2 mW) was directed perpendicularly upon the sample. Two polarizers (P1 in x direction and P2 in y direction) were placed before and behind the grating. Light experiences a polarization change due to the birefringence property of the LC existing in the grating. The sample can be rotated in the x-y plane, and α is the angle between the grating vector and the y direction. The birefringence result will be further used in our model to determine the degree of phase separation. A precise characterization of DE was also carried out here, and we carefully controlled the setup to ensure light was incident onto the same spot as in the birefringence measurement to avoid error caused by in homogeneity of the grating.

3. Results and Discussion

A. Nondroplet Morphology

Compared with the solid isotropic polymer matrix, the physical property of phase-separated LC is more difficult obtain. In order to explain the diffractive properties of the transmission grating quantitatively and to understand the LC features, three issues are addressed by our research: the form of phase-separated LC existing in the grating (droplet or pure slice), the alignment of phase-separated LC in the grating, and the amount of the phase-separated LC. Figure 3(a) gives a POM image of one sample grating with a period of 3 μm. The grating shows a morphology consisting of isotropic polymer walls separated by sharp-edged LC films. The surface topology of the transmission grating with narrower grating pitch is shown in Fig. 3(b). The surface of the grating shows a sinusoidal-type profile, and there have been no irregularities caused by the presence of LC droplet domains [26]. Therefore we confirm the phase-separated LC has the form of pure slices instead of droplets. The previous research [20] dealing with the relation between the grating morphology and monomer functionality indicates that the non droplet scaffolding morphology is a result of low-functionality acrylate monomer. This seems to be in conflict with the high-functionality acrylate DPHPA monomer employed in this study (in fact, the droplet-like morphology has been observed in gratings using DPHPA), but if the low illumination intensity is taken into consideration, we may infer that low polymerization rate is the fundamental reason for the scaffolding morphology. Indeed, in [27] the model used by the authors to explain the POLICRYPS-forming mechanism indicates that there are two regimes (fast-curing regime and slow-curing regime) to obtain good gratings. The POLICRYPS and scaffolding gratings fall in the slow-curing regime using different methods: one by increasing monomer diffusion, the other by lowering down the polymerization rate, respectively.

B. Rotation of LC Director during Fabrication

Figure 4 shows the real-time change of diffraction efficiency for differently polarized light. For clarity we

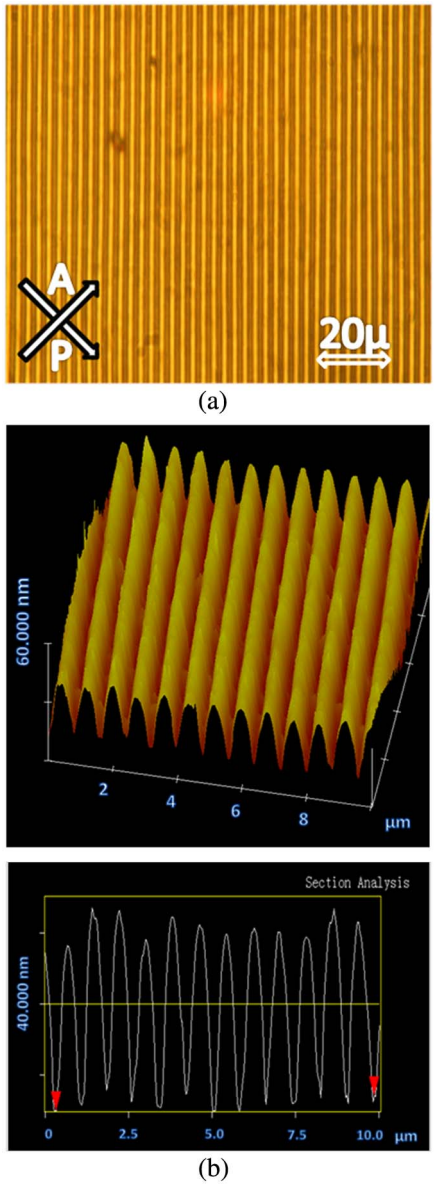

(a)

(b)

Fig. 3. (Color online) Scaffolding morphology: (a) POM image of the grating. Polarizer and analyzer axes are oriented in the image. Fringe spacing $\Lambda = 3$ μm. (b) AFM profiles of the transmission grating. Fringe spacing $\Lambda = 0.78$ μm.

adopt a coordinate system with x in the direction of the grating vector and z perpendicular to the cell surface. The diffraction efficiency for each polarization at the Bragg angle [28] can be written as

$$\eta_p = \sin^2 \frac{\pi L(\cos^2 \theta_B \varepsilon_{1x} - \sin^2 \theta_B \varepsilon_{1z})}{\lambda_0 2\overline{n} \cos \theta_B}, \quad (1)$$

$$\eta_s = \sin^2 \frac{\pi L \varepsilon_{1y}}{\lambda_0 2\overline{n} \cos \theta_B}. \quad (2)$$

Here $\varepsilon_{1i}(i = x, y, z)$ is the diagonal components of the relative permittivity modulation tensor, λ_0 is the wavelength of the probe light (633 nm), $\overline{n}$ is the average refractivity of the grating, θ_B is the Bragg angle,

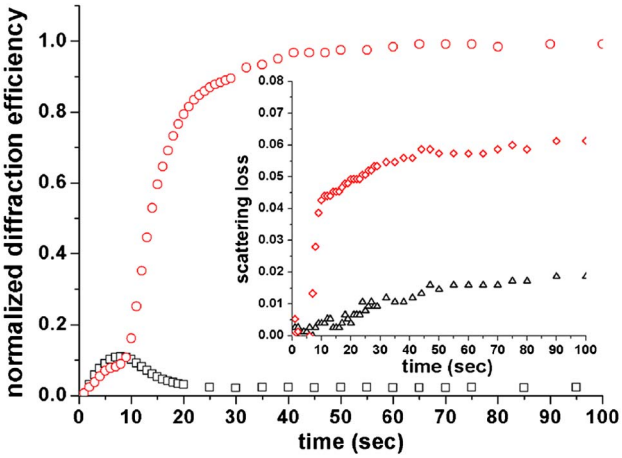

Fig. 4. (Color online) The evolution of normalized diffraction efficiency for p polarization (open circle) and s polarization (open square) with time. The inset shows the evolution of scattering loss for p polarization (open diamond) and s polarization (open triangle) with time.

and L is the film thickness. As the value of θ_B is small (15.2° in this experiment), Eqs. (1) and (2) can be simplified as

$$\eta_p \approx \sin^2 \frac{\pi L \varepsilon_{1x}}{\lambda_0 2\bar{n}}, \tag{3}$$

$$\eta_s \approx \sin^2 \frac{\pi L \varepsilon_{1y}}{\lambda_0 2\bar{n}}. \tag{4}$$

From Eqs. (3) and (4), we note that η_p increases with the amount of phase-separated LC and the extent to which the LC is aligned along the x axis (because $n_{\text{pure polymer}} = 1.532$, measured by an Abbe refractometer, is close to the ordinary refractive index of LC), and η_s increases with the amount of phase-separated LC and the extent to which LC is aligned along the y axis. At the first stage of the reaction (<8 seconds), both η_p and η_s increase with time. This is because the small amount of LC in the dark regions is still miscible with monomers and there is no LC ordering at the beginning of the phase-separation process [29,30]. Then at $t = 8$ s, the LC in the dark regions is no longer miscible with monomers and starts to phase separate to form pure LC. The simultaneous changes in the DE curve (a much faster increase for η_p and a decrease for η_s) could be related to the fact that the phase-separated LC begins to align along the x axis. Grating optical sensitivity η_p/η_s at the final stage is greater than 50. This value is in distinct contrast to that for droplet-like morphology ($\eta_p/\eta_s \approx 5$), and can be thought as a symbol of a fairly good alignment of LC along the grating vector.

Generally speaking, scattering arises from scattering domains. Two requirements are needed to define a scattering domain. One is that its refractive index has a mismatch with the environment, and the other is that its size is comparable to incident light wavelength. So there have been two ways to decrease scattering loss in HPDLC gratings: one is to decrease the LC droplet size [22,31], which requires an extremely fast polymerization rate, and the other is to avoid the formation of LC droplets, as is the case with POLICRYPS or scaffolding morphology gratings. Figure 4 (inset) is the scattering loss change with reaction time in a scaffolding morphology grating, in which the occurrence of scattering light is almost in synchronization with the phase separation. This is understandable as the phase separation will inevitably bring some scattering domains [23]. The scattering loss is much lower than typical droplet-like morphology grating [15,16]. We also note the scattering loss for p polarization (seeing n_e in the LC) is larger than that for s polarization (seeing n_o in the LC) caused by a greater refractive index mismatch.

C. Amount of Phase-Separated LC

For droplet-like morphological gratings, no convincing quantity of phase-separated LC was given, and this parameter was treated as a fitting parameter to fit diffractive curves in previous research. The uncertainty about the size distribution of LC droplets, uncertainty about the LC alignment inside the microsized LC droplets, and uncertainty about the mean director of the LC droplets make quantitative characterization difficult. Here, in order to clear the amount of phase-separated LC in the scaffolding morphological grating, we use optical birefringence measurement to determine the amount of the pure, aligned, phase-separated LC. According to Jones matrices formalism [32], the transmission for both vertically aligned polarizers and horizontally aligned polarizers through the sample in Fig. 2 can be written as

$$I(\alpha)_{\perp} = I_{\text{OT}} \sin^2\left(\frac{\varphi}{2}\right) \sin^2(2\alpha), \tag{5}$$

$$I(\alpha)_{\parallel} = I_{\text{OT}} \left[1 - \sin^2\left(\frac{\varphi}{2}\right)\right] \sin^2(2\alpha). \tag{6}$$

Here α is the angle between the grating vector and the y axis, and φ is the retardation phase of the grating. Based on Eq. (5), if the phase-separated LC is aligned along the grating vector, $I(\alpha)_{\perp}$ achieves maximum value at $\alpha = 45°$. Our measurement showed the actual $\alpha_{I_{\perp(\max)}} = 45° \pm 1°$, which means the LC is well aligned along the grating vector. The small tilt of the mean LC director from the grating vector will be neglected in our calculation. We further obtain phase retardation φ using Eqs. (5) and (6):

$$\varphi = 2 \arcsin \sqrt{\frac{I(45°)_{\perp}}{I(45°)_{\perp} + I(45°)_{\parallel}}} \tag{7}$$

Therefore the average sample birefringence can be written as

$$\Delta n = \frac{\lambda \varphi}{2\pi L}. \tag{8}$$

Here λ is the wavelength of the probe light (633 nm) and L is the film thickness.

For the same sample as in section B, experimentally we have $I(45°)_{\perp} = 340$ and $I(45°)_{\parallel} = 345$. The average sample birefringence is calculated using Eq. (8) as 0.0242. As the polymer matrix appears isotropic and will cause no phase retardation, the amount of phase-separated LC in the whole mixture is 14.25 wt.% by $\Delta n/(n_e - n_o)$. Considering the initial LC percent in the mixture, the phase-separation degree of this grating β is 41.93%. We note that the value of β here is not the highest we can achieve because with different scaffolding gratings, shown in Table 1, we obtained values as high as 70%. Next we will demonstrate that the birefringence measurement is a reliable tool to quantify the phase-separated LC in the scaffolding morphology.

D. Diffraction Efficiency

According to the AFM image in Fig. 3, the phase-separated LC takes the form of a periodic sinusoidal wave, and it is reasonable for us to assume the relative permittivity of the two-phase grating is changing sinusoidally with x as shown in Fig. 5. Calculus calculation shows the relative permittivity modulation tensor ε_{1i} can be expressed as

$$\varepsilon_{1i} = \frac{\pi}{4}(S_1 - S_2). \tag{9}$$

Here S_1 and S_2 are the average relative permittivity of regions 1 and 2, respectively.

From the experimental results and discussions in sections A, B, and C, the two-phase grating can be regarded as a pure LC layer (though with some monomers dissolved in it, as will be discussed afterwards; we already have calculation proof that this part has a negligible influence over the final results, and we can regard this part as just a pure LC layer) and the polymer matrix with some LC dissolved in it. To obtain the average relative permittivity of regions 1 and 2, we assume the dissolved LC distribution across the polymer is homogenous and the relative permittivity of the polymer matrix can be expressed as

Table 1. Summary of DE for Different Samples[a]

Λ (nm)	η_p	η_s	η_p^*	η_s^*
1279	94.6%	95.8%	4.4%	3.7%
1027	90.8%	90.5%	6.3%	4.0%
778	75.2%	76.5%	2.0%	2.5%
681	71.8%	74.9%	2.1%	2.5%
607	85.8%	88.6%	3.7%	3.1%
532	33.2%	32.9%	0.5%	1.1%

[a] η_p and η_s are experimental data; η_p^* and η_s^* are calculated values by the model.

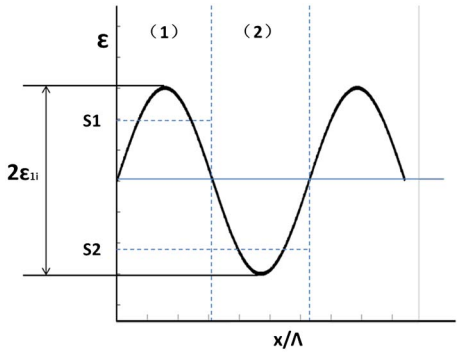

Fig. 5. (Color online) Schematic sinusoidal curve for relative permittivity.

$$\varepsilon_p = \frac{2n_o^2 + n_e^2}{3}\frac{0.34 - \beta}{1 - \beta} + n_{\text{pure polymer}}^2 \frac{0.66}{1 - \beta}. \tag{10}$$

Here β is the percent of phase-separated LC in the whole mixture. $n_{\text{pure polymer}}$ is measured by an Abbe refractometer using a monomer mixture. S_1 and S_2 can be expressed as

$$S_1 = 2\beta\langle\varepsilon_{\text{LC}}\rangle + (1 - 2\beta)\varepsilon_p, \tag{11}$$

$$S_2 = \varepsilon_p. \tag{12}$$

Putting Eqs. (10), (11), and (12) into Eq. (9) for the sample studied in section B and C, we have

$$\langle\varepsilon_{1i}\rangle = \begin{bmatrix} 0.107 & 0 & 0 \\ 0 & -0.0146 & 0 \\ 0 & 0 & -0.0146 \end{bmatrix} \tag{13}$$

Once the information of the transmission grating is obtained, we can use the anisotropic coupled-wave theory to quantitatively explain the diffractive properties. Shown in Fig. 6. is the dependence of DE for p-polarized light on the deviation angle from its Bragg angle. The solid line is the calculation result using the anisotropic coupled-wave theory; no fitting parameter is used. As the DE for s-polarized light is too small to been shown in an angular dependence curve, we just give its maximum DE, η_s(calculation) = 2.5% and η_s(experimental) = 2.0%. The agreement between calculation data and experimental data is fairly good, and we quantitatively show the strong dependence of DE on the polarization of the incident light is a result of the well-aligned, pure phase-separated LC layer, and the use of birefringence measurement to determine the amount of phase-separated LC in the scaffolding morphology transmission grating is effective and efficient.

To further prove the effectiveness of this method, we apply it to randomly selected samples with different grating pitch and phase-separation degree. It is worth mentioning that all samples were cured under similar low illumination intensity to ensure the

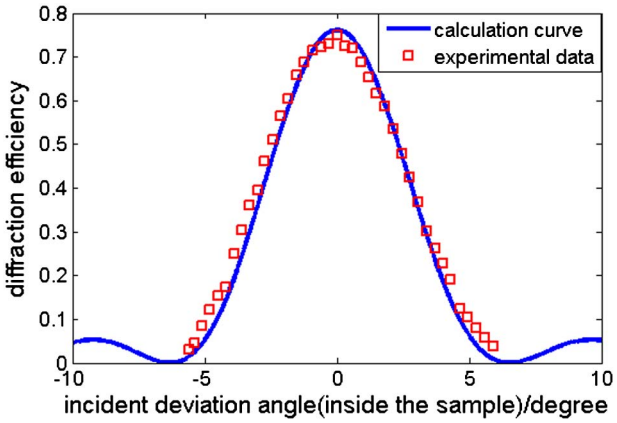

Fig. 6. (Color online) DE of the transmission grating for p-polarized light as a function of the deviation incident angle from the Bragg angle. Curve: calculation data. Open square: experimental data.

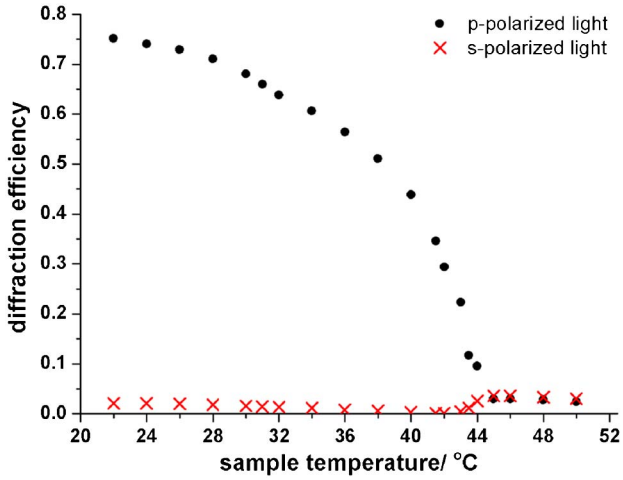

Fig. 7. (Color online) Temperature dependence of DE. Black circle: p-polarized light. Red cross: s-polarized light.

scaffolding morphology. The upper limit of the grating pitch is chosen as 1279 nm to ensure the Q factor of the transmission is greater than 10 [33], in which regime the coupled-wave theory can give good results. Results are summarized in Table 1; the agreement is fairly good. Experientially, phase-separation degree is more complete for samples with a larger grating pitch; the steep intersecting angle for a narrow grating period may be the reason. Besides, optimum recording intensity varies with grating pitch: a narrow grating tends to need a comparatively stronger recording light. For application purpose, with proper curing parameters and cell thickness, all these non droplet-morphology gratings can exhibit high DE for p-polarized light (95%).

E. Temperature Dependence

To further gain a deeper understanding of the grating structure, the dependence of DE for each polarization on temperature is studied. The sample was mountedon a heating stage with a thermocouple embedded in it. Each temperature was kept constant with an accuracy of 0.1° C. Results are shown in Fig. 7. The temperature dependence for s-wave DE reveals an interesting non monotonic behavior, though the DE is rather small. At low temperature, the s wave experiences $n_0 = 1.522$ in the well-aligned phase-separated LC and $n_p = 1.543$ in the polymer matrix. As temperature increases, the well-aligned LC gradually undergoes a transition to the isotropic state; then the s wave experiences a refractive index between 1.522 and 1.58. There is a moment when the s wave experiences a refractive index of 1.543 in the pure LC, and the grating property vanishes. So the non monotonic behavior of the s wave comes from good alignment of phase-separated LC along the grating vector.

When temperature is higher than 45 °C, the grating isoptically isotropic and the transition temperature is lower than that of the pure LC. We further carried on some independent experiments by measuring the clearing point of the LC with some monomer dissolved in it, and found about 5% dissolved monomer can be responsible for the reduced clearing point. The DE calculation error caused by the dissolved monomer is around 1%, so the above calculation does not take the 5% monomer into account. Based on the data in sections B, C, and D, we can predict the DE for the s wave at the temperature above the clearing point. The calculated value is 7%. Though the error caused by LC and polymer thermal refractive index coefficients is small, it is still two times greater than the actual value, 3%, and that is why we did not use the DE above the clearing point to determine the degree of phase separation.

4. Conclusions

In this paper, we carried out a systematic optical characterization of the HPDLC transmission grating with scaffolding morphology made from high-functionality acrylate monomer, which consists of almost pure LC films separated by polymer matrix with the LC director homogeneously aligned along the grating vector. We determined the phase-separation degree by birefringence measurement. Results showed this grating can exhibit high DE, low scattering loss, and a high degree of phase separation. We explained the diffractive properties using anisotropic coupled-wave theory without any fitting parameter. The agreement between theory and experimental data was fairly good for samples with different fringe spacing and phase-separation degree. The forming mechanism of the scaffolding morphology transmission grating may be the same as with POLICRYPS, as they both fall in the slow-curing regime, one through slowing down the polymerization rate with low curing intensity, the other through enhancing the monomer diffusion by heating.

Though these two kinds of gratings show similar physical properties with a pure LC layer and homogenously aligned LC director, they also hold some peculiar properties. First, the ordinary index of LC is closer to that of cured polymer using acrylate

monomers than those using thiol-ene adhesive, so the scaffolding morphology grating diffractive properties are more sensitive to light polarization; this high anisotropic property has already been demonstrated as applicable [34]. Second, the phase-separated LC in the scaffolding morphology undergoes an additional interaction with the polymer filaments. This interaction influences the alignment of the LC. We have already demonstrated LC alignment could be changed by utilizing this anchoring strength [35]. Meanwhile, this interaction makes electric driving difficult. We found the critical field of the scaffolding morphology grating is 3 V/μm and the turn-off field is about 12 V/μm, which is much higher than for POLICRYPS. The response time is much faster as the anchoring strength will assist the LC in relaxing back to its original state. We believe this low scattering, highly anisotropic, efficient phase-separation HPDLC component will attract renewed interest and be exploited for applications in various fields.

The authors would like to thank the support from the Natural Science Foundation of China (grant Nos. 60578035, 50473040, and 60736042).

References

1. K. Pavani, I. Naydenova, J. Raghavendra, S. Martin, and V. Toal, "Electro-optical switching of the holographic polymer-dispersed liquid crystal diffraction gratings," J. Opt. A **11**, 024023 (2009).
2. L. H. Domash, T. Chen, B. N. Gomatam, C. M. Gozewski, R. L. Sutherland, L. V. Natarajan, V. P. Tondiglia, T. J. Bunning, and W. W. Adams, "Switchable-focus lenses in holographic polymer-dispersed liquid crystal," Proc. SPIE **2689**, 188–194 (1996).
3. H. Jashnsaz, N. H. Nataj, E. Mohajerani, and A. Khabbazi, "All-optical switchable holographic Fresnel lens based on azo-dye-doped polymer-dispersed liquid crystals," Appl. Opt. **50**, 4295–4301 (2011).
4. M. S. Park, E. H. Kim, and B. K. Kim, "Applications of holographic PDLC for full color display," J. Polym. Eng. **28**, 169–178 (2008).
5. R. Jakubiak, T. J. Bunning, R. A. Vaia, L. V. Natarajan, and V. P. Tondiglia, "Electrically switchable, one-dimensional polymeric resonators from holographic photopolymerization: a new approach for active photonic bandgap materials," Adv. Mater. **15**, 241–244 (2003).
6. V. K. S. Hisao, C. Lu, G. S. He, M. Pan, A. N. Cartwright, P. N. Prasad, R. Jakubiak, R. A. Vaia, and T. J. Bunning, "High contrast switching of distributed-feedback lasing in dye-doped H-PDLC transmission grating structures," Opt. Express **13**, 3787–3794 (2005).
7. Y. J. Liu, X. W. Sun, H. I. Elim, and W. Ji, "Effect of liquid crystal concentration on the lasing properties of dye-doped holographic polymer-dispersed liquid crystal transmission gratings," Appl. Phys. Lett. **90**, 011109 (2007).
8. R. L. Sutherland, L. V. Natarajan, and V. P. Tondiglia, "Bragg gratings in an acrylate polymer consisting of periodic polymer-dispersed liquid-crystal planes," Chem. Mater. **5**, 1533–1538 (1993).
9. M. Jazbinšek, I. D. Olenik, and M. Zgonik, "Characterization of holographic polymer dispersed liquid crystal transmission gratings," J. Appl. Phys. **90**, 3831–3837 (2001).
10. R. L. Sutherland, "Polarization and switching properties of holographic polymer-dispersed liquid-crystal gratings. I. Theoretical model," J. Opt. Soc. Am. B **19**, 2995–3003 (2002).
11. I. Drevenšek-Olenik, M. Fally, and M. A. Ellabban, "Temperature dependence of optical anisotropy of holographic polymer-dispersed liquid crystal transmission gratings," Phys. Rev. E **74**, 021707 (2006).
12. F. Vita, D. E. Lucchetta, R. Castagna, L. Criante, and F. Simoni, "Effects of resin addition on holographic polymer dispersed liquid crystals," J. Opt. **11**, 024021 (2009).
13. T. J. White, W. B. Liechty, L. V. Natarajan, V. P. Tondiglia, T. J. Bunning, and C. A. Guymon, "The influence of *N*-vinyl-2-pyrrolidinone in polymerization of holographic polymer dispersed liquid crystals (HPDLCs)," Polymer **47**, 2289–2298 (2006).
14. J. M. Wofford, L. V. Natarajan, V. P. Tondiglia, R. L. Sutherland, P. F. Lloyd, S. A. Siwecki, and T. J. Bunning, "Holographic polymer dispersed liquid crystal (HPDLC) transmission gratings formed by visible light initiated thiol-ene photopolymerization," Proc. SPIE **6332**, 63320Q (2006).
15. R. L. Sutherland, L. V. Natarajan, V. P. Tondiglia, T. J. Bunning, and W. W. Adams, "Electrically switchable volume gratings in polymer-dispersed liquid crystals," Appl. Phys. Lett. **64**, 1074–1076 (1994).
16. R. Caputo, L. De Sio, A. Veltri, C. Umeton, and A. V. Sukhov, "Development of a new kind of switchable holographic grating made of liquid-crystal films separated by slices of polymeric material," Opt. Lett. **29**, 1261–1263 (2004).
17. L. De Sio, N. Tabiryan, R. Caputo, A. Veltri, and C. Umeton, "POLICRYPS structures as switchable optical phase modulators," Opt. Express **16**, 7619–7624 (2008).
18. R. Caputo, A. De Luca, L. De Sio, L. Pezzi, G. Strangi, C. Umeton, A. Veltri, R. Asquini, A. d'Alessandro, D. Donisi, R. Beccherelli, A. V. Sukhov, and N. V. Tabiryan, "POLICRYPS: a liquid crystal composed nano/microstructure with a wide range of optical and electro-optical applications," J. Opt. **11**, 024017 (2009).
19. K. K. Vardanyan, J. Qi, J. N. Eakin, M. D. Sarkar, and G. P. Crawford, "Polymer scaffolding model for holographic polymer-dispersed liquid crystals," Appl. Phys. Lett. **81**, 4736–4738 (2002).
20. M. D. Sarkar, N. L. Gill, J. B. Whitehead, and G. P. Crawford, "Effect of monomer functionality on the morphology and performance of the holographic transmission gratings recorded on polymer dispersed liquid crystals," Macromolecules **36**, 630–638 (2003).
21. R. L. Sutherland, L. V. Natarajan, V. P. Tondiglia, S. Chandra, C. K. Shepherd, D. M. Brandelik, S. A. Siwecki, and T. J. Bunning, "Polarization and switching properties of holographic polymer-dispersed liquid-crystal gratings. II. Experimental investigations," J. Opt. Soc. Am. B **19**, 3004–3012 (2002).
22. F. Vita, A. Marino, V. Tkachenko, G. Abbate, D. E. Lucchetta, L. Criante, and F. Simoni, "Visible and near-infrared characterization and modeling of nanosized holographic-polymer-dispersed liquid crystal gratings," Phys. Rev. E **72**, 011702 (2005).
23. R. L. Sutherland, V. P. Tondiglia, L. V. Natarajan, P. F. Lloyd, and T. J. Bunning, "Coherent diffraction and random scattering in thiol-ene-based holographic polymer-dispersed liquid crystal reflection gratings," J. Appl. Phys. **99**, 123104 (2006).
24. R. Caputo, A. Veltri, C. Umeton, and A. V. Sukhov, "Kogelnik-like model for the diffraction efficiency of POLICRYPS gratings," J. Opt. Soc. Am. B **22**, 735–742 (2005).
25. M. Xu, L. De Sio, R. Caputo, Cesare P. Umeton, Arthur J. H. Wachters, Dick K. G. de Boer, and H. Paul Urbach, "Characterization of the diffraction efficiency of polymer-liquid-crystal-polymer-slices gratings at all incidence angles," Opt. Express **16**, 14532–14543 (2008).
26. M. D. Sarkar, J. Qi, and G. P. Crawford, "Influence of partial matrix fluorination on morphology and performance of HPDLC transmission graings," Polymer **43**, 7335–7344 (2002).
27. A. Veltri, R. Caputo, C. Umeton, and A. V. Sukhov, "Model for the photoinduced formation of diffraction gratings in liquid-crystalline composite materials," Appl. Phys. Lett. **84**, 3492–3494 (2004).
28. J. J. Butler, M. S. Malcuit, and M. A. Rodriguez, "Diffractive properties of highly birefringent volume gratings: investigation," J. Opt. Soc. Am. B **19**, 183–189 (2002).

29. R. L. Sutherland, V. P. Tondiglia, and L. V. Natarajan, "Evolution of anisotropic reflection gratings formed in holographic polymer-dispersed liquid crystals," Appl. Phys. Lett. **79**, 1420–1422 (2001).
30. S. Harbour, J. V. Kelly, T. Galstian, and J. T. Sheridan, "Optical birefringence and anisotropic scattering in acrylate based holographic polymer dispersed liquid crystals," Opt. Commun. **278**, 28–33 (2007).
31. D. E. Lucchetta, R. Karapinar, A. Manni, and F. Simoni, "Phase-only modulation by nanosized polymer-dispersed liquid crystals," J. Appl. Phys. **91**, 6060–6065 (2002).
32. M. Born and E. Wolf, *Principles of Optics* (Pergamon, 1980).
33. H. Kogelnic, "Coupled wave theory for thick hologram gratings," Bell Syst. Tech. J. **69**, 2909–2946 (1969).
34. Z. Zheng, F. Guo, Y. Liu, and L. Xuan, "Low threshold and high contrast polymer dispersed liquid crystal grating based on twisted nematic polarization modulator," Appl. Phys. B **91**, 17–20 (2008).
35. W. Huang, S. Deng, W. Li, Z. Peng, Y. Liu, L. Hu, and L. Xuan, "A polarization-independent and low scattering transmission grating for a distributed feedback cavity based on holographic polymer dispersed liquid crystal," J. Opt. **13**, 085501 (2011).